

Optical analysis of spherical mirrors of telescopes: the lens-less Schmidt case

Paolo W. Cattaneo*

INFN Pavia, Via Bassi 6 - 27100, Pavia, Italy

Abstract

The light distribution on the focal surface of spheric mirrors designed for telescopes in the lens-less Schmidt configuration is calculated analytically using geometrical optics.

This analysis was motivated by considerations of the design the design of the AUGER fluorescence detector [1]. Its geometrical parameters are used in the examples.

1. Introduction

The lens-less Schimdt configuration employs a circular diaphragm at the center of curvature of the mirror. In this configuration the coma aberration is a second order effect and the dominant aberration is spherical.

We are interested in calculating the light distribution on the focal surface of the spherical mirror. This information is relevant for an optimal design of the mirror and for use in detector simulation.

In Fig.1 a schematic of the mirror is drawn. The adimensional normalized

*Corresponding author

Email address: Paolo.Cattaneo@pv.infn.it (Paolo W. Cattaneo)

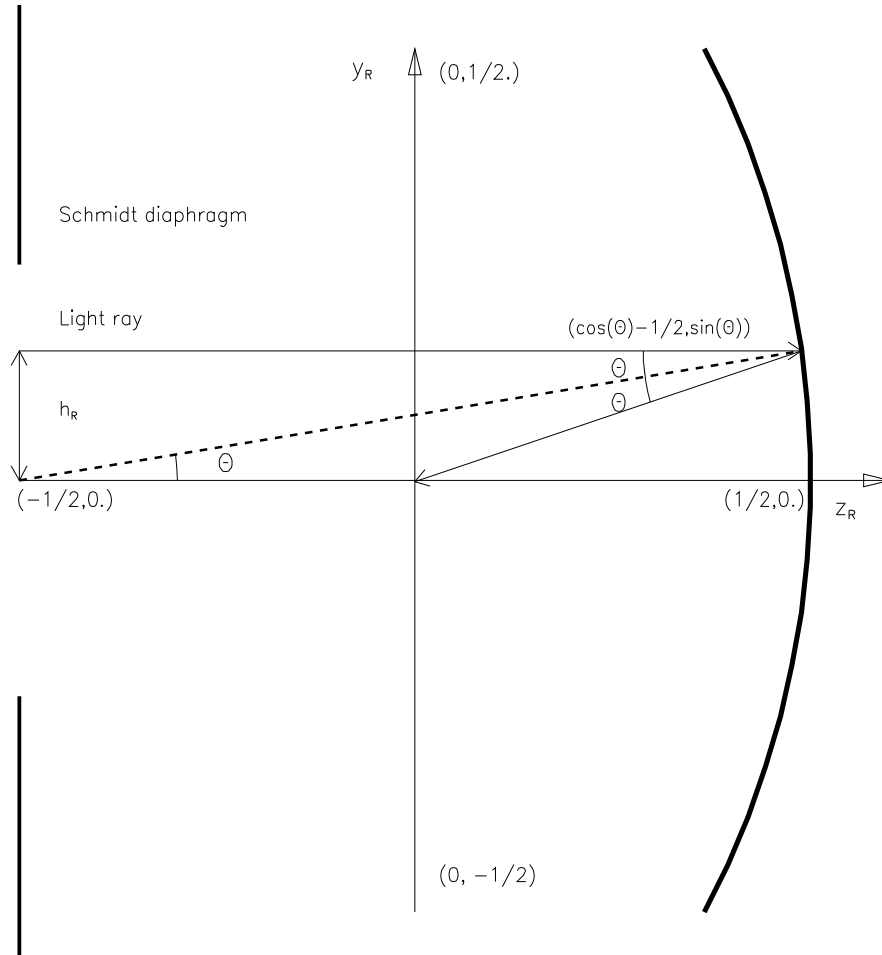


Figure 1: Schematic of the mirror with the reference coordinate system.

coordinates $z_R = \frac{z}{R_M}$, $y_R = \frac{y}{R_M}$ and $\rho_R = \frac{\rho}{R_M}$ are introduced.

The mirror is spherical with curvature radius $R_M = 3400$ mm and size 3500 mm \times 3500 mm .

The light entrance is limited by a circular diaphragm located at the mirror center of curvature with a semiaperture $R_d = 850$ mm that defines an opening angle $\sin \Theta_M = R_d/R_M$.

The light distribution on and close to the focal surface due to paraxial rays is calculated below including the effect of camera obscuration.

2. Light distribution from paraxial rays without obscuration

We consider a ray parallel to the z_R axis at radial distance $h_R = h/R_M \leq R_d/R_M$. In Fig.1, the ray lies in the $y_R - z_R$ plane.

The ray intercepts the mirror at the point $((\cos \Theta - \frac{1}{2}), \sin \Theta)$ where Θ is the angle with respect to the circle center (not the axis origin). The reflected ray forms an angle 2Θ with the z_R axis. Its equation in cylindrical coordinates $\rho_R z_R$ is

$$\begin{aligned} \rho_R - \sin \Theta &= \tan 2\Theta \left(z_R - \left(\cos \Theta - \frac{1}{2} \right) \right) \\ \rho_R &= \tan 2\Theta \left(z_R + \frac{1}{2} \left(1 - \frac{1}{\cos \Theta} \right) \right) \end{aligned} \quad (1)$$

2.1. Calculation of the caustic

The calculation of the light distribution on the focal surface requires the knowledge of the caustic of the spherical surface. The relevant formulae are in the Appendix.

The relevance of the caustic stems from the fact that, for $\sin \Theta \leq \sin \Theta_M$, it is

the outer envelope of the converging rays. We are interested in studying the behavior of the rays close to the focal surface, where the previous condition on Θ is satisfied. Hence, the outer diameter of the light disk $\rho_R(z_R)$ is the maximum between the radial coordinates of the caustic and of the rays from the mirror rim, that is Eq.1 for $\Theta = \Theta_M$.

2.2. Light envelope and disk of minimal confusion

The size and the intensity of the light envelope are calculated by reformulating the equation of the caustic and solving the following system:

$$\begin{aligned} z_R &= \frac{1}{2} \left[-1 + \sqrt{1 - \rho_R^{\frac{2}{3}}(1 + 2\rho_R^{\frac{2}{3}})} \right] \\ \rho_R &= \tan 2\Theta_M \left(z_R + \frac{1}{2} \left(1 - \frac{1}{\cos \Theta_M} \right) \right) \end{aligned} \quad (2)$$

The solution is anticipated to be at $|\rho_R| \ll 1$, therefore the approximation in Eq.14 in the Appendix can be applied, resulting in the following third order polynomial equation:

$$z_R^3 - \frac{27}{64} \tan^2(2\Theta_M) \left[z_R^2 + z_R \left(1 - \frac{1}{\cos \Theta_M} \right) + \frac{1}{4} \left(1 - \frac{1}{\cos \Theta_M} \right)^2 \right] = 0. \quad (3)$$

Eq.3 can be solved with the Cardano method.

The reflected ray from the largest angle Θ_M (mirror rim or diaphragm limited circle) intersects the caustic at two points. It is tangent at larger z_R , by definition of the caustic, and has a simple intersection at smaller z_R . At this point the radius of the light envelope is minimum. This is the disk of minimal confusion, given by

$$p = -\frac{27}{64} \tan^2 2\Theta_M \left[\left(1 - \frac{1}{\cos \Theta_M}\right) + \frac{9}{64} \tan^2 2\Theta_M \right]$$

$$q = \frac{2}{27} \left[-\frac{27}{64} \tan^2 2\Theta_M \right]^3 - \frac{1}{3} \left[-\frac{27}{64} \tan^2 2\Theta_M \right]^2 \left(1 - \frac{1}{\cos \Theta_M}\right) - \frac{27}{64} \tan^2 2\Theta_M \left(1 - \frac{1}{\cos \Theta_M}\right)^2$$

$$z_{Rdm} = \sqrt[3]{-\frac{q}{2} + \sqrt{\frac{p^3}{27} + \frac{q^2}{4}}} + \sqrt[3]{-\frac{q}{2} - \sqrt{\frac{p^3}{27} + \frac{q^2}{4}}} + \frac{9}{64} \tan^2(2\Theta_M) \quad (4)$$

In Fig.2 the envelope of light rays near the mirror focus is pictured together with the caustic and a bundle of rays reflected from the mirror. The outer envelope is given by the rays converging from the outer rim for

$$\frac{1}{2}(-1 + \sqrt{1 - \sin^2 \Theta_M}(1 + 2 \sin^2 \Theta_M)) \leq z_R$$

and by the caustic for

$$z_{Rdm} \leq z_R \leq \frac{1}{2}(-1 + \sqrt{1 - \sin^2 \Theta_M}(1 + 2 \sin^2 \Theta_M))$$

and by the rays diverging from the outer rim for

$$z_R \leq z_{Rdm}$$

where z_{Rdm} is the position of the disk of minimal confusion obtained by Eq.3. The radius of the outer envelope versus the radial distance is displayed in Fig.3 (solid line) for $R_M = 3400$ mm. The envelope contains all the light reflected from the mirror.

The position of the disk of minimal confusion is $R = 1742.52$ mm and its radius 7.32 mm.

In [2]-[3], the AUGER design is analyzed using both user-written and professional ray tracing programs. The most straightforward comparison with these calculations is with [3] where exactly the same geometrical parameters are used. The positions of the focal surface and the radius of the disk of minimal confusion agree within ≈ 0.1 mm.

2.3. Light distribution

The radial light distribution $\frac{df}{d\rho_R}$ at fixed z_R is obtained by relating the known light distribution in h_R to that in ρ_R . The relation stems from

$$\frac{df}{d\rho_R} = \frac{df}{d\Theta} \frac{d\Theta}{d\rho_R} = \frac{df}{dh_R} \frac{dh_R}{d\Theta} \frac{d\Theta}{d\rho_R} = \frac{df}{dA} \frac{dA}{dh_R} \frac{dh_R}{d\Theta} \frac{d\Theta}{d\rho_R} \quad (5)$$

The first factor is the inverse of the effective area of the mirror $\frac{df}{dA} = (\pi R_M^2 \sin^2 \Theta_M)^{-1}$, the second is simply $\frac{dA}{dh_R} = 2\pi R_M^2 h_R$ and the third is from $h_R = \sin \Theta$, $\frac{dh_R}{d\Theta} = \cos \Theta$. The fourth is derived by differentiating Eq.1

$$\frac{d\Theta}{d\rho_R} = \frac{1}{\frac{2}{\cos^2 2\Theta} (z_R + \frac{1}{2}(1 - \frac{1}{\cos \Theta})) - \frac{\tan 2\Theta \sin \Theta}{2 \cos^2 \Theta}}.$$

Substituting in Eq.5 we find

$$\frac{df}{d\rho_R} = \frac{\sin 2\Theta}{\sin^2 \Theta_M} \frac{1}{\frac{2}{\cos^2 2\Theta} (z_R + \frac{1}{2}(1 - \frac{1}{\cos \Theta})) - \frac{\tan 2\Theta \sin \Theta}{2 \cos^2 \Theta}} \quad (6)$$

where Θ is expressed as a function of ρ_R by inverting Eq.1.

If more than one $\Theta(\rho_R)$ satisfies Eq.1, the right side of Eq.6 becomes the sum of all the solutions.

The inversion requires the canonical change of variable $t = \tan \Theta/2$. In this variable $\sin \Theta = \frac{2t}{1+t^2}$ and $\cos \Theta = \frac{1-t^2}{1+t^2}$, so that Eq.1 becomes

$$t^4 + \frac{4(z_R + 1)}{\rho_R} t^3 - 6t^2 - \frac{4z_R}{\rho_R} t + 1 = 0 \quad (7)$$

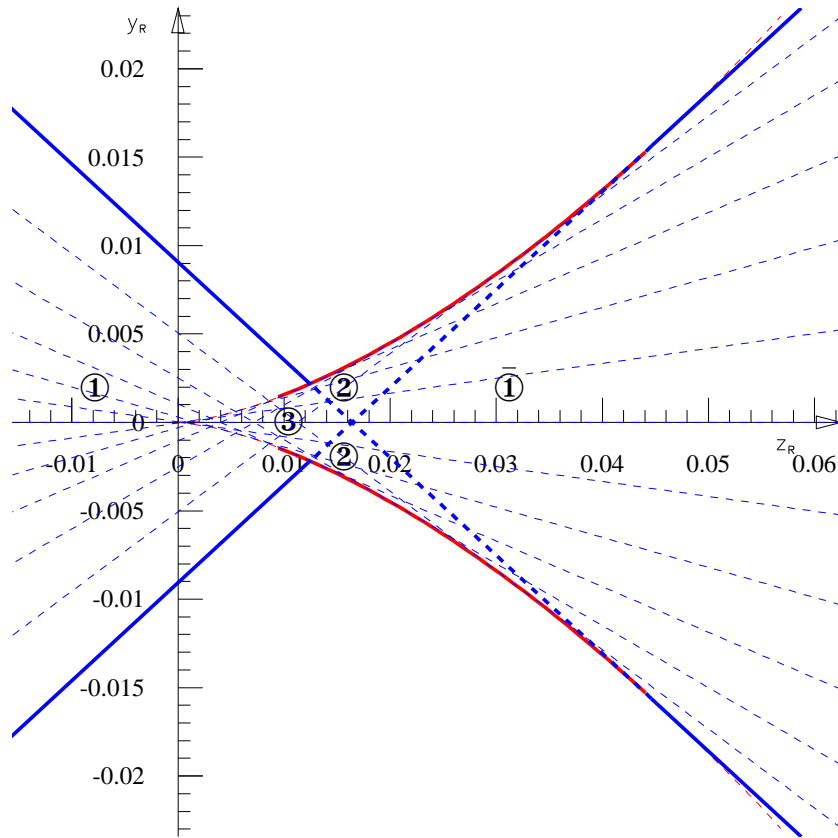


Figure 2: Envelope of light rays near the focus without obscuration. Thick lines are external, dashed internal.

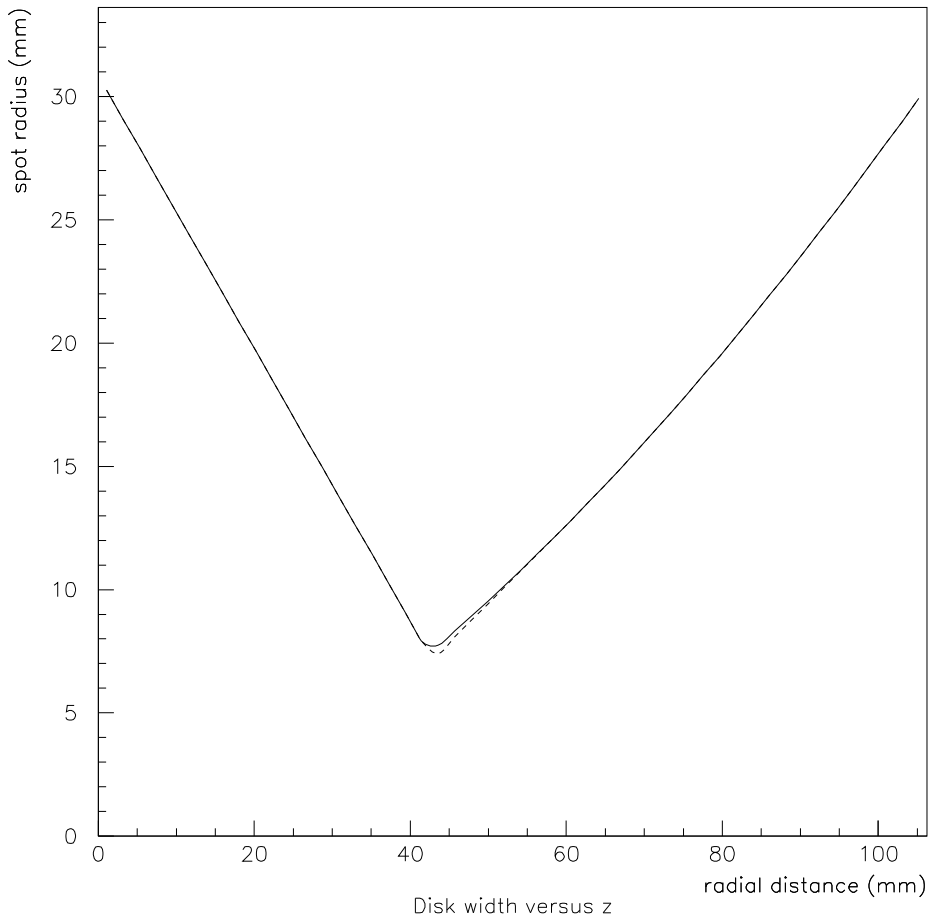


Figure 3: Spot radius versus radial distance from the focus: unobscured case (solid), obscured case (dashed).

This equation has 4 complex solutions and it is guaranteed that an even number of them are real although that might appear counterintuitive when Fig.2 is analyzed graphically.

In the region (marked with ③ in Fig.2) within the caustic and within the rays from the mirror rim after their crossing, three rays meet at a given ρ_R . One is converging at small Θ and has not yet reached the caustic, one is converging at larger Θ and has already reached the caustic and one is diverging at even larger and opposite sign Θ and has already reached the caustic on the opposite site.

In the region (marked with ② in Fig.2) within the caustic and outside the rays from the mirror rim, there are two rays, the diverging ray is missing.

In the region (marked with $\overline{\textcircled{1}}$ in Fig.2) within the caustic and within the rays from the mirror rim before their crossing, there is only the converging ray that has not yet reached the caustic.

In the region (marked with $\textcircled{1}$ in Fig.2) outside the caustic and within the rays from the mirror rim after their crossing, there is only the diverging ray that has already reached the caustic.

In the region outside the caustic and outside the rays from the mirror rim, there are no rays.

The reason for this apparent contradiction is that Eq.7 for $\rho_R > 0$ always has one solution for $t \leq -1$, that is $\Theta \leq -\pi/2$, and vice versa for $\rho_R < 0$. That corresponds to a ray refracted (not reflected) by an unphysical hemisphere specular image around the ρ_R axis of the physical one. In other words, Eq.1 represents full straight lines, while the reflected rays are only half straight lines. This solution is unphysical and must be neglected.

Analysis of Eq.7 leads to the conclusion that, for $\rho_R > 0$, there is always an

additional real solution for $-1 < t < 0$ and a pair of solutions that can be either both real positive or complex conjugates.

The reason for the presence of a region with two solutions is that the solution at large and opposite sign Θ lays outside the physical region $(-\Theta_M, \Theta_M)$. The same reason requires the region with one solution of converging ray at small Θ .

In these two regions and in the region with three physical solutions, Eq.7 has four real solutions. In the region with one physical solution outside the caustic, Eq.7 has two real and two complex solutions.

Eq.7 can be solved exactly using the canonical Ferrari approach. Yet the solution is very cumbersome and provides little insight into its physical meaning. The unphysical solution for the refracted ray can be removed since the ratio of the second to the fourth terms is $6/t^2$, where, at most, $t = \tan \Theta_M/2 \approx \Theta_M/2 \approx 1/8$. This ratio is at least 384 and dropping the fourth power term will affect the physical solutions only by a very small amount. With this approximation, Eq.7 becomes

$$t^3 - \frac{6\rho_R}{4(z_R + 1)}t^2 - \frac{z_R}{(z_R + 1)}t + \frac{\rho_R}{4(z_R + 1)} = 0 \quad (8)$$

The radial distribution $\frac{df}{d\rho_R}$ is plotted in Fig.4. The two-dimensional distribution is plotted in Fig.5.

They are in good agreement with the light distributions shown in [2]-[3].

3. Light distribution from paraxial rays with obscuration

In the AUGER design there is a $0.92 \times 0.92 \text{ m}^2$ photomultiplier camera with a spherical surface next to the mirror focal surface, that obscures a

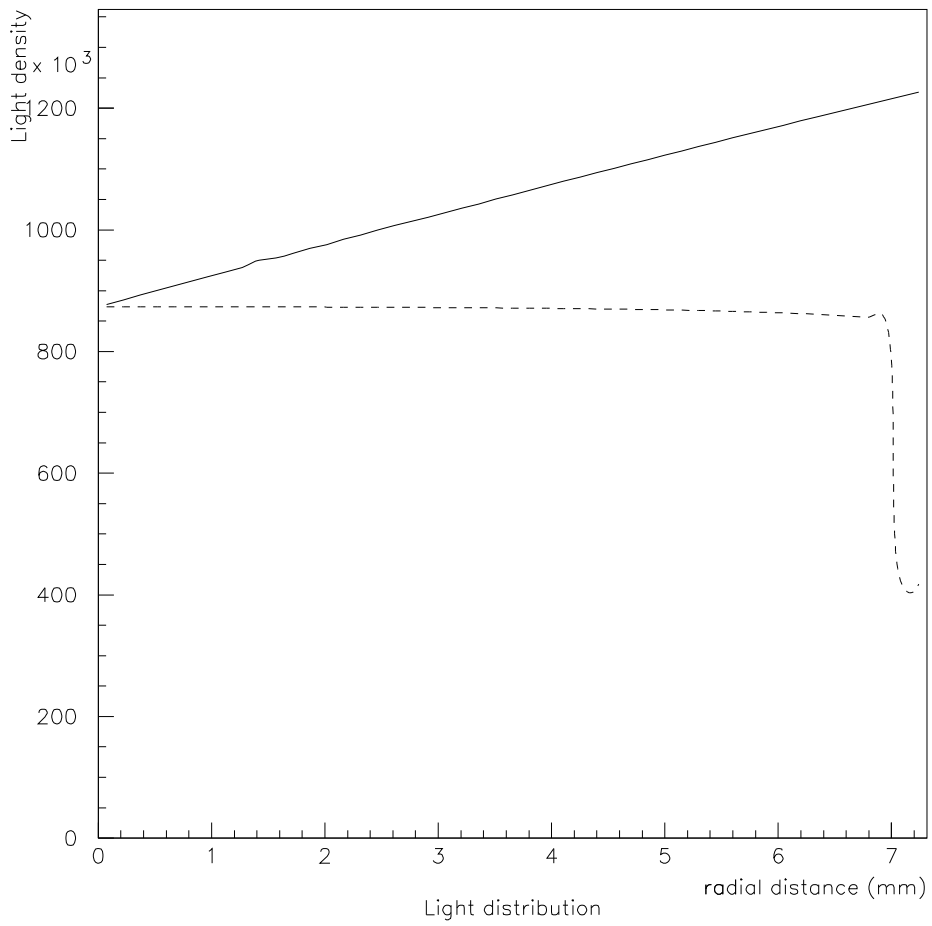


Figure 4: Radial light distribution at the disk of least confusion for unobscured (solid) and obscured (dashed) cases

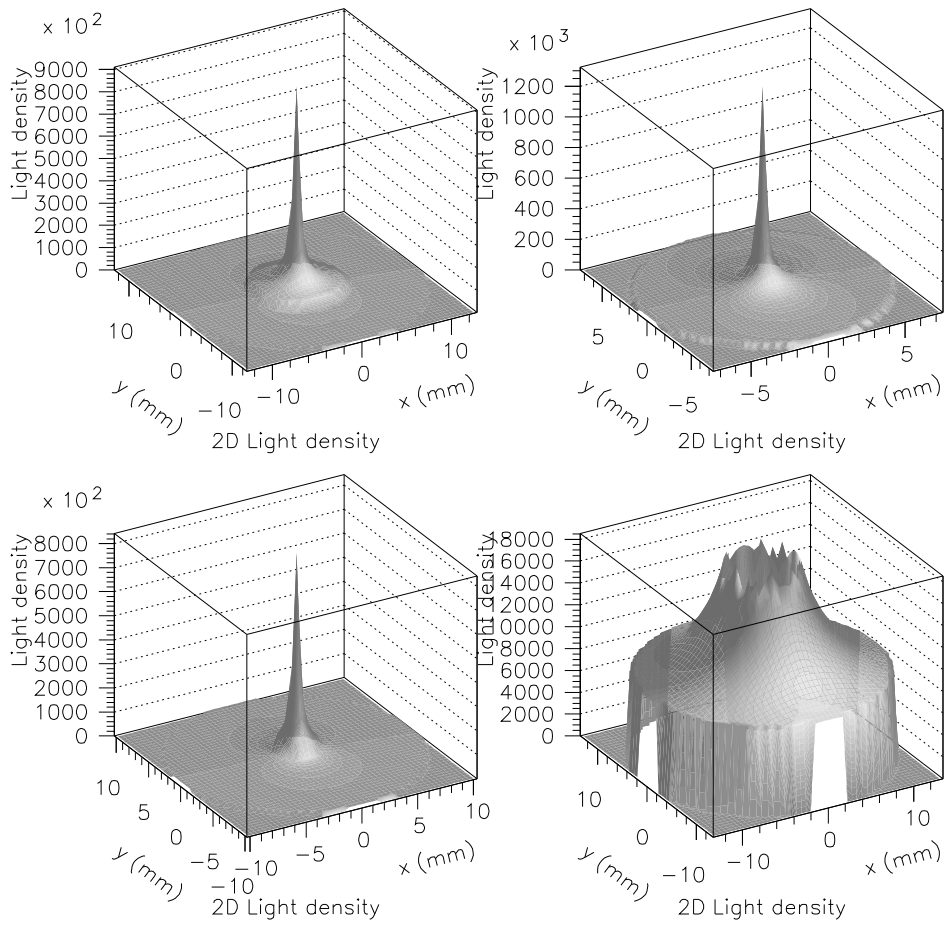


Figure 5: Two dimensional light distributions at $-10, 0, +10, +20$ mm from the plane of least confusion

fraction of the incoming rays.

The camera does not have rotational symmetry but its obscuration can be approximated by a disk with the same area, that is with radius $R_c = 0.519$ m positioned next to the focal surface $z_R = 1/2$. That implies that the rays hit the mirror only for angle $\sin \Theta \geq \sin \Theta_c = R_c/R_M$, that is for $\Theta \geq \Theta_c = 8.78^\circ$.

3.1. Light envelope and disk of minimal confusion

The obscuration changes the light distribution along z_R and might change the size and position of the disk of minimal confusion. The outer envelope of reflected light can be deduced by referring to Fig.6 and noting that the light rays close to the z_R axis are obscured. Hence the outer light envelope is given by the converging rays from the mirror rim up to the caustic, then by the caustic, then, possibly, by the converging rays from the rim of the obscuration disk, then by the diverging rays from the mirror rim.

It depends on the obscuration area if the converging rays from the rim of the obscuration disk intersect the caustic at $z_{Rc}(\Theta_c)$ before or after $z_{Rdm}(\Theta_M)$ from Eq.4, that is if

$$z_{Rdm}(\Theta_M) \geq \frac{1}{2}(-1 + \sqrt{1 - \sin^2 \Theta_c(1 + 2 \sin^2 \Theta_c)}) \approx \frac{3}{4} \sin^2 \Theta_c = z_{Rc}(\Theta_c)$$

where the caustic approximation of Eq.14 is used.

Therefore if $\sin \Theta_c \leq \sqrt{z_{Rdm}(\Theta_M)4/3}$, the outer envelope is unchanged, otherwise for $z_{Rdm} < z_R < z_{Rc}$ it is given by the converging rays from the rim of the obscuration disk. In this case the disk of minimal confusion is obtained by the intersection of the diverging ray from the outer rim with the converging one on the opposite side from the rim of the obscuration disk. The result is

$$\begin{aligned}
z_{Rdm} &= \frac{1}{2} \left(-1 + \left(\frac{\tan 2\Theta_M}{\cos \Theta_M} + \frac{\tan 2\Theta_c}{\cos \Theta_c} \right) \frac{1}{\tan 2\Theta_c + \tan 2\Theta_M} \right) \\
\rho_{Rdm} &= \frac{\tan 2\Theta_c}{2} \left(\left(\frac{\tan 2\Theta_c}{\cos \Theta_M} + \frac{\tan 2\Theta_c}{\cos \Theta_c} \right) \frac{1}{\tan 2\Theta_M + \tan 2\Theta_c} - \frac{1}{\cos \Theta_c} \right) 9)
\end{aligned}$$

This condition is verified in the AUGER design and the location of the disk of minimal confusion changes slightly. Its position is $R = 1742.80$ mm and its radius is 7.17 mm. The radius of the envelope versus the radial distance for the obscured case is displayed in Fig.3 (dashed line). The difference between it and that of the unobscured case is minimal.

3.2. Light distributions

The results of the unobscured case are still valid, provided that only solutions with $\Theta_c \leq |\Theta| \leq \Theta_M$ are considered.

The radial light distributions for the obscured case is presented in Fig.4 .

4. Conclusions

Detailed analytical calculations of the spherical aberration of a telescope spherical mirror designed for detecting fluorescence light emitted in the atmosphere by extended air showers generated by very high energy cosmic ray interactions are presented. The position of the focal surface of the mirror and the light distribution on and close to it have been calculated. The calculations are useful both for the design of the detector and for the detector simulation. The AUGER Fluorescence Detector has been used as example but the results are applicable to any similar detector.

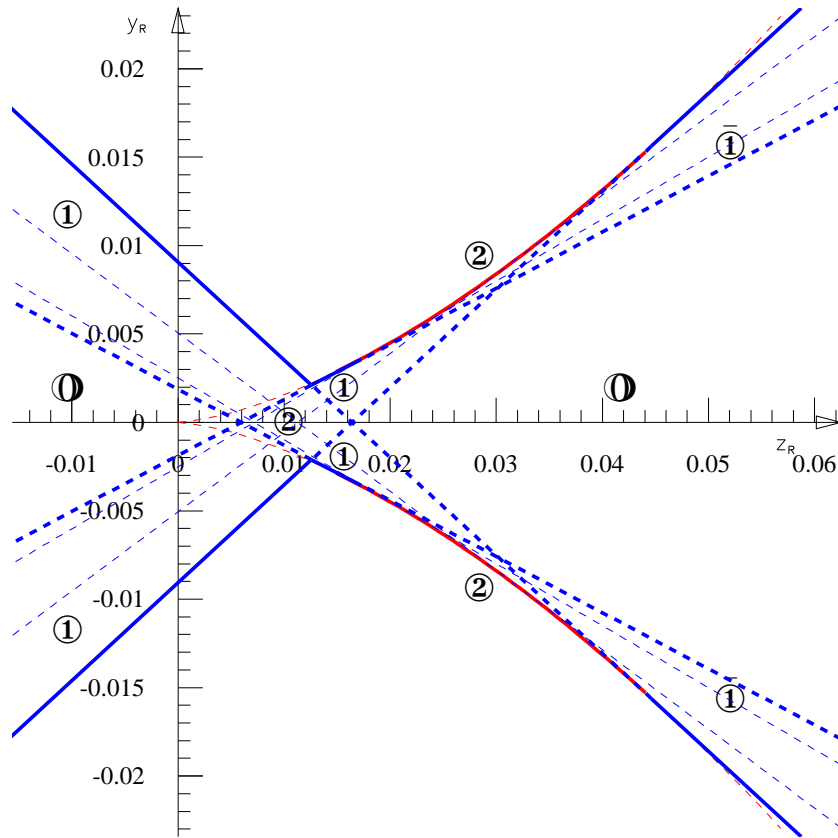


Figure 6: Envelope of light rays next to the focus with obscuration. Thick lines are external, dashed internal.

Appendix

Third order equation

We recall the solution of the third order polynomial equation. The original equation and the intermediate steps leading to the solution x_1 , x_2 and x_3 are listed (where $\omega = \sqrt[3]{1}$, $\omega \neq 1$)

$$\begin{aligned}
 0 &= x^3 + a_1x^2 + a_2x + a_3 \\
 p &= a_2 - \frac{a_1^2}{3} \quad q = \frac{2a_1^3}{27} - \frac{a_1a_2}{3} + a_3 \\
 P &= \sqrt[3]{-\frac{q}{2} + \sqrt{\frac{p^3}{27} + \frac{q^2}{4}}} \\
 Q &= \sqrt[3]{-\frac{q}{2} - \sqrt{\frac{p^3}{27} + \frac{q^2}{4}}} \\
 x_1 &= P + Q - \frac{a_1}{3} \quad x_2 = \omega P + \omega^2 Q - \frac{a_1}{3} \quad x_3 = \omega^2 P + \omega Q - \frac{a_1}{3} \quad (10)
 \end{aligned}$$

Two roots coincides if and only if $\frac{p^3}{27} + \frac{q^2}{4} = 0$. In this case, the third distinct root is x_1 , that is the solution determining the disk of least confusion in our application.

Some formulae about the caustic

The calculation of the analytical form of the caustic from a spherical surface is a standard calculation, but it is surprisingly difficult to find it in text books. Following [4], the caustic is the locus of intersection of neighbouring reflected rays when their distance becomes infinitesimal. Referring to the coordinate system in Eq.1 and using the dimensionless variables $z_R = \frac{z}{R_M}$ and $y_R = \frac{y}{R_M}$, it can be calculated by equating the derivative of Eq.1 with respect to Θ to 0 and solving the system

$$\begin{aligned}
y_R &= \tan 2\Theta \left(z_R + \frac{1}{2} \left(1 - \frac{1}{\cos \Theta} \right) \right) \\
0 &= \frac{2}{\cos^2 2\Theta} \left(z_R + \frac{1}{2} \left(1 - \frac{1}{\cos \Theta} \right) \right) - \frac{1 \tan 2\Theta \tan \Theta}{2 \cos \Theta}
\end{aligned} \tag{11}$$

The resulting curve can be expressed in parametric form as

$$\begin{aligned}
y_R(\Theta) &= \sin^3 \Theta \\
z_R(\Theta) &= \frac{1}{2}(-1 + \sqrt{1 - \sin^2 \Theta}(1 + 2 \sin^2 \Theta))
\end{aligned} \tag{12}$$

The caustic in three dimensions is obtained by rotating the curve in Eq.12 around the z_R axis.

It is useful to express exactly the caustic in alternative forms as $z_R(y_R)$, $y_R(z_R)$ and relating the parameter Θ to y_R and z_R . From Eq.12,

$$\begin{aligned}
\Theta(y_R) &= \arcsin(\sqrt[3]{y_R}) \\
z_R(y_R) &= \frac{1}{2}(-1 + \sqrt{1 - y_R^{2/3}}(1 + 2y_R^{2/3})).
\end{aligned} \tag{13}$$

A common and useful approximation for $|\sin \Theta| \ll 1$ (equivalent to $|y_R| \ll 1$ and $|z_R| \ll 1$) is obtained from $\sqrt{1 - y_R^{2/3}} \approx 1 - \frac{1}{2}y_R^{2/3}$, that implies

$$\begin{aligned}
z_R(y_R) &= \frac{3}{4}y_R^{2/3} \\
y_R(z_R) &= \pm \left(\frac{4z_R}{3} \right)^{3/2} \\
\Theta(z_R) &= \pm \arcsin \left(\sqrt{\frac{4z_R}{3}} \right)
\end{aligned} \tag{14}$$

The exact expression for $y_R(z_R)$ or, equivalently, for $\Theta(z_R)$ is obtained from Eq.12 by writing

$$z_R(\Theta) = \frac{1}{2}(-1 + \cos \Theta(3 - 2 \cos^2 \Theta))$$

which can be reformulated as a third order polynomial equation in $\cos \Theta$

$$\cos^3 \Theta - \frac{3}{2} \cos \Theta + (z_R + \frac{1}{2}) = 0.$$

The discriminant of this equation is

$$\Delta = -\frac{1}{8} + \frac{1}{4}(z_R + \frac{1}{2})^2$$

which is negative for $-\frac{\sqrt{2}+1}{2} < z_R < \frac{\sqrt{2}-1}{2} = z_{R0}$. For these values, there are three real solutions:

$$\begin{aligned} \cos \Theta_1(z_R) &= \sqrt{2} \cos \left(\frac{3\pi + \arctan \left(\frac{\sqrt{2-4(z_R+\frac{1}{2})^2}}{2(z_R+\frac{1}{2})} \right)}{3} \right) \\ \cos \Theta_2(z_R) &= \sqrt{2} \cos \left(\frac{5\pi + \arctan \left(\frac{\sqrt{2-4(z_R+\frac{1}{2})^2}}{2(z_R+\frac{1}{2})} \right)}{3} \right) \\ \cos \Theta_3(z_R) &= \sqrt{2} \cos \left(\frac{\pi + \arctan \left(\frac{\sqrt{2-4(z_R+\frac{1}{2})^2}}{2(z_R+\frac{1}{2})} \right)}{3} \right) \end{aligned} \quad (15)$$

The physical meaning of these solutions can be understood by considering them for $z_R = 0$

$$\begin{aligned} \cos \Theta_1(0) &= \sqrt{2} \cos \left(\frac{11}{12} \pi \right) = -\frac{\sqrt{2}}{2} \sqrt{2 + \sqrt{3}} \\ \cos \Theta_2(0) &= \sqrt{2} \cos \left(\frac{\pi}{4} \right) = 1 \\ \cos \Theta_3(0) &= \sqrt{2} \cos \left(\frac{5}{12} \pi \right) = \frac{\sqrt{2}}{2} \sqrt{2 - \sqrt{3}} \end{aligned} \quad (16)$$

The first is unphysical because the modulus is larger than one, the second corresponds to the tip of the caustic and the third is a large angle solution. Depending on the quadrant, the solutions are always monotonic versus z_R either increasing (Θ_1 and Θ_3) or decreasing (Θ_2) within the range $-\frac{1}{2} \leq z_R \leq z_{R0}$. The lower bound of the range is physical, the upper one comes from requiring three real solutions. For $z_R = z_{R0}$, $\Theta_2 = \Theta_3 = \pi/4$ and for $z_R > z_{R0}$, Θ_2 and Θ_3 become complex conjugate.

The solution relevant for the application to a mirror is therefore Θ_2 and we can write the exact parametrization of the caustic for $0 \leq z_R \leq z_{R0}$

$$\Theta(z_R) = \pm \arccos \left(\sqrt{2} \cos \left(\frac{5\pi + \arctan\left(\frac{\sqrt{2-4(z_R+\frac{1}{2})^2}}{2(z_R+\frac{1}{2})}\right)}{3} \right) \right)$$

$$y_R(z_R) = \pm \left(-\cos 2 \left(\frac{5\pi + \arctan\left(\frac{\sqrt{2-4(z_R+\frac{1}{2})^2}}{2(z_R+\frac{1}{2})}\right)}{3} \right) \right)^{\frac{3}{2}}$$

The large angle solution is Θ_3 and reads

$$\Theta(z_R) = \pm \arccos \left(\sqrt{2} \cos \left(\frac{\pi + \arctan\left(\frac{\sqrt{2-4(z_R+\frac{1}{2})^2}}{2(z_R+\frac{1}{2})}\right)}{3} \right) \right)$$

$$y_R(z_R) = \pm \left(-\cos 2 \left(\frac{\pi + \arctan\left(\frac{\sqrt{2-4(z_R+\frac{1}{2})^2}}{2(z_R+\frac{1}{2})}\right)}{3} \right) \right)^{\frac{3}{2}}$$

Acknowledgments

We warmly acknowledge Prof. William Molzon from the Department of Physics and Astronomy of the University of California, Irvine, CA, USA, for

his careful proofreading of the manuscript.

References

- [1] J. Abraham et al. Properties and performance of the prototype instrument for the Pierre Auger Observatory. *Nucl. Instr. and Meth.*, A533:50–95, 2004.
- [2] G. Matthiae and P. Privitera. The Schmidt telescope with corrector plane. GAP-98-039.
http://www.auger.org/admin/GAP_Notes/GAP1998/GAP_98_039.ps.gz.
- [3] M. Hrabovsky et al. The optical analysis of the proposed schmidt camera design. GAP-99-025.
http://www.auger.org/admin/GAP_Notes/GAP1999/GAP_99_025.pdf.
- [4] B. Rossi. *Ottica*, chapter 2.7. Masson Italia Editori, Milano, 1984.